doi:10.1038/nature20173

Hypoxia induces heart regeneration in adult mice

Yuji Nakada[1]*, Diana C. Canseco[1]*, SuWannee Thet[1], Salim Abdisalaam[2], Aroumougame Asaithamby[2], Celio X. Santos[3], Ajay M. Shah[3], Hua Zhang[4], James E. Faber[4], Michael T. Kinter[5], Luke I. Szweda[5], Chao Xing[6], Zeping Hu[7], Ralph J. Deberardinis[7], Gabriele Schiattarella[1], Joseph A. Hill[1], Orhan Oz[8], Zhigang Lu[9], Cheng Cheng Zhang[9], Wataru Kimura[1,10] & Hesham A. Sadek[1,11]

The adult mammalian heart is incapable of regeneration following cardiomyocyte loss, which underpins the lasting and severe effects of cardiomyopathy. Recently, it has become clear that the mammalian heart is not a post-mitotic organ. For example, the neonatal heart is capable of regenerating lost myocardium[1], and the adult heart is capable of modest self-renewal[2,3]. In both of these scenarios, cardiomyocyte renewal occurs via the proliferation of pre-existing cardiomyocytes, and is regulated by aerobic-respiration-mediated oxidative DNA damage[4,5]. Therefore, we reasoned that inhibiting aerobic respiration by inducing systemic hypoxaemia would alleviate oxidative DNA damage, thereby inducing cardiomyocyte proliferation in adult mammals. Here we report that, in mice, gradual exposure to severe systemic hypoxaemia, in which inspired oxygen is gradually decreased by 1% and maintained at 7% for 2 weeks, results in inhibition of oxidative metabolism, decreased reactive oxygen species production and oxidative DNA damage, and reactivation of cardiomyocyte mitosis. Notably, we find that exposure to hypoxaemia 1 week after induction of myocardial infarction induces a robust regenerative response with decreased myocardial fibrosis and improvement of left ventricular systolic function. Genetic fate-mapping analysis confirms that the newly formed myocardium is derived from pre-existing cardiomyocytes. These results demonstrate that the endogenous regenerative properties of the adult mammalian heart can be reactivated by exposure to gradual systemic hypoxaemia, and highlight the potential therapeutic role of hypoxia in regenerative medicine.

Zebrafish, urodele amphibians, and immature mammals are capable of myocardial regeneration following various types of injury, mediated primarily through the proliferation of pre-existing cardiomyocytes[1,6–8]. Given that most cardiomyocytes in mammals exit cell cycle shortly after birth, induction of cell cycle re-entry of adult cardiomyocytes has emerged as a central focus for cardiac regeneration.

Mitochondrial-derived reactive oxygen species (ROS) represent a major source of oxidative stress in post-natal cardiomyocytes[9]. We recently demonstrated that the transition from the hypoxic intrauterine environment to the post-natal environment induces cardiomyocyte cell cycle arrest through mitochondrial ROS-induced oxidative DNA damage[4]. Moreover, cycling cardiomyocytes in the adult mammalian heart are hypoxic, and thus are protected from oxidative DNA damage[5]. These studies suggest that oxygen-dependent mitochondrial metabolism is a major driver of cell cycle arrest of cardiomyocytes. However, it is not known whether changes in ambient oxygen affect cardiomyocyte cell cycle in adult mammals.

Here we show that chronic severe hypoxaemia, induced by a gradual reduction in inspired oxygen, reduces ROS and oxidative DNA damage in the cardiomyocytes. Importantly, this was sufficient to induce cell cycle re-entry of adult cardiomyocytes, which resulted in significant functional recovery following myocardial infarction (MI). Although counterintuitive, these results suggest that targeting this pathway could be a viable strategy for mammalian heart regeneration.

In order to examine the effect of systemic hypoxia on mitochondrial metabolism, we exposed mice to low oxygen tension (7% O_2) for 2 weeks. To avoid hypobaropathy caused by a rapid drop in partial oxygen pressure[10], we gradually dropped the fraction of inspired oxygen (FiO_2) by 1% per day from 20.9% (room air oxygen) to 7% over the course of 2 weeks followed by exposure to 7% oxygen for an additional 2 weeks (Fig. 1a). We observed a reduction in food intake during hypoxia exposure (Extended Data Fig. 1a), therefore the normoxic mice were given an equivalent amount of food. Blood gas analysis of the normoxic mice were found to be within normal levels previously reported in anaesthetized rodents[11]. As expected, arterial pH in hypoxic mice was markedly decreased, and arterial pO_2 was decreased. Moreover, pCO_2 level was decreased in the hypoxia group, probably owing to hyperventilation (respiratory compensation) (Extended Data Fig. 1b). Two days following exposure to 7% oxygen, stabilization of hypoxia inducible factor 1 α subunit (Hif1α) in cardiomyocytes was observed as indicated by an increase in the number of fluorescent protein tdTomato$^+$ cardiomyocytes in αMHC-CreERT2-ODD;R26/tdTomato double transgenic mice[5] (Extended Data Fig. 1c). The acute increase in tdTomato$^+$ cardiomyocytes seen here was due to hypoxic stabilization of Hif1α rather than cardiomyocyte expansion. Following 2 weeks of hypoxia exposure, we observed a significant decrease in mitochondrial cristae density (Fig. 1b) and in cardiac mitochondrial DNA copy number (Fig. 1c). Mass spectrometry-based quantification of enzymes involved in mitochondrial Krebs cycle and fatty acid β-oxidation provided further support for the reduction in mitochondrial metabolism in hypoxic hearts (Fig. 1d, Extended Data Fig. 1d). Moreover, unsupervised analysis of metabolite levels demonstrated a significant effect of hypoxia on cardiomyocyte metabolome. For example, hypoxic hearts accumulated 2-hydroxyglutarate, as previously reported in hypoxic cancer cells[12], as well as numerous metabolites associated with hypoxia such as 5-aminolevulinic acid[13], allantoin[14], dihydroorotate[15], betaine[16], creatine[16] and a reduction in several TCA cycle metabolites, as expected for states of reduced oxidative metabolism[17] (Extended Data Figs 2 and 3). In addition, an NADH oxidase assay demonstrated that mitochondrial electron transport chain activity was markedly decreased in the hypoxic hearts (Fig. 1e).

[1]Department of Internal Medicine, University of Texas Southwestern Medical Center, Dallas, Texas 75390, USA. [2]Department of Radiation Oncology, University of Texas Southwestern Medical Center, Dallas, Texas 75390, USA. [3]Cardiovascular Division, King's College London BHF Centre of Research Excellence, Faculty of Medicine, James Black Centre, London SE5 9NU, UK. [4]Department of Cell Biology and Physiology, McAllister Heart Institute, the University of North Carolina, Chapel Hill, North Carolina 27599-7545, USA. [5]Free Radical Biology and Aging Research Program, Oklahoma Medical Research Foundation, Oklahoma City, Oklahoma 73104, USA. [6]McDermott Center for Human Growth and Development, University of Texas Southwestern Medical Center, Dallas, Texas 75390, USA. [7]Children's Medical Center Research Institute at UT Southwestern Medical Center, Dallas, Texas 75390, USA. [8]Department of Radiology, University of Texas Southwestern Medical Center, Dallas, Texas 75390, USA. [9]Department of Physiology and Developmental Biology, University of Texas Southwestern Medical Center, Dallas, Texas 75390, USA. [10]Life Science Center, Tsukuba Advanced Research Alliance, University of Tsukuba, 1-1-1 Tennoudai, Tsukuba, Ibaraki 305-8577, Japan. [11]Center for Regenerative Science and Medicine, University of Texas Southwestern Medical Center, Dallas, Texas 75390, USA.
*These authors contributed equally to this work.

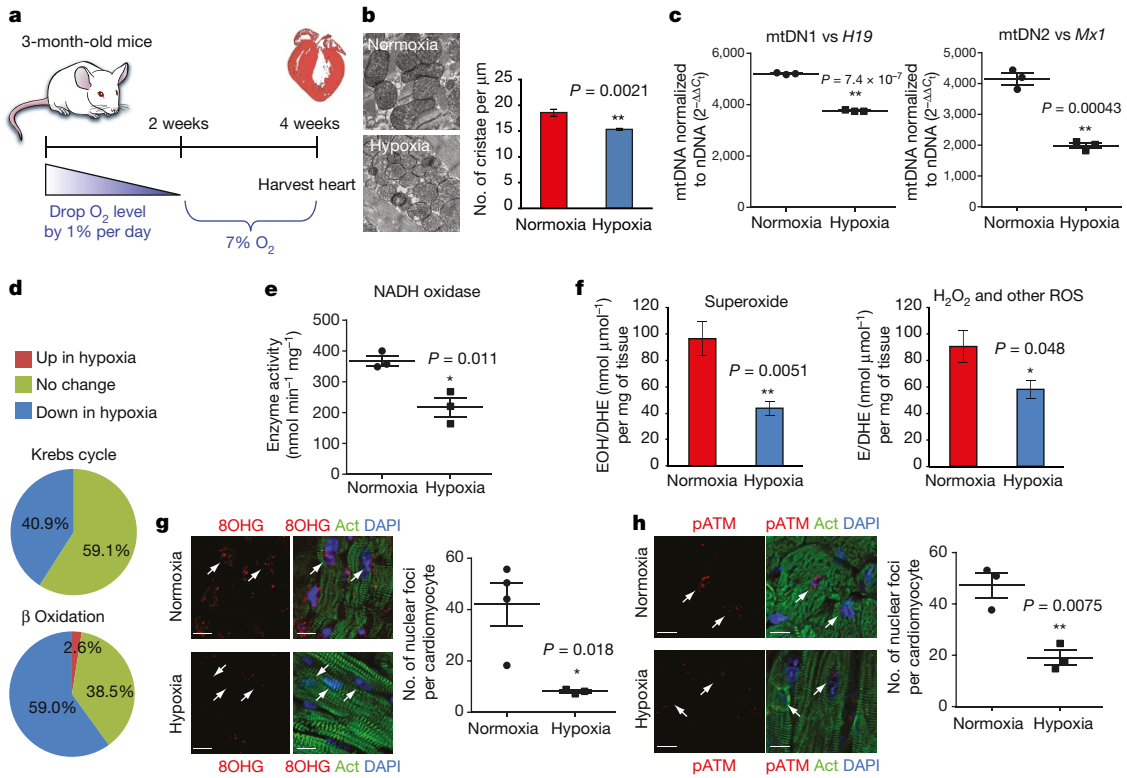

Figure 1 | Chronic hypoxia exposure leads to decreased mitochondrial ROS and decreased oxidative DNA damage in cardiomyocytes. **a**, Schematic of gradual induction of severe hypoxaemia. **b**, Transmission electron microscopy images of mitochondria in ventricular cardiomyocytes and quantification of average number of cristae per μm showed a significantly less dense cristae structure in cardiomyocytes in the hypoxia-exposed heart ($n = 5$ each). **c**, Quantitative PCR analysis of mitochondrial DNA showed that mitochondrial DNA copy number normalized to nuclear DNA copy number (mtDN1 versus H19 or mtDN2 versus Mx1) was significantly decreased following hypoxia exposure ($n = 3$ each). **d**, Quantitative mass spectrometry analysis showed that a large proportion of enzymes involved in mitochondrial Krebs cycle and fatty acid β oxidation were significantly decreased following hypoxia exposure ($n = 3$ each; values rounded to the nearest decimal place). **e**, The enzymatic activity of NADH oxidase (normalized to mitochondrial protein) showed a significant decrease in electron transport chain activity following chronic hypoxia exposure ($n = 3$ each). **f**, High performance liquid chromatography-based measurement of superoxide (left side), and H_2O_2 and other ROS (right side) both indicated a significant decrease in ROS level in the heart after an exposure to hypoxia ($n = 5$ each). **g**, Immunofluorescence using anti-8OHG antibody showed a significant decrease in oxidative DNA damage in cardiomyocytes from hypoxia-treated mice ($n = 4$ for normoxia, and 3 for hypoxia). **h**, Immunofluorescence using an anti-phosphorylated-ATM antibody showed a significant decrease in the activation of DNA damage response pathway in cardiomyocytes from hypoxia-treated hearts ($n = 3$ each). Scale bars, 10 μm. Data are presented as mean ± s.e.m. $^*P < 0.05$, $^{**}P < 0.01$.

Assessment of ROS fluorescence in fresh tissue sections demonstrated that hypoxia results in a marked reduction in ROS fluorescence (Extended Data Fig. 1e), and high-performance liquid-chromatography-based measurement of superoxide and H_2O_2 showed a significant decrease of ROS in hypoxic hearts (Fig. 1f). This resulted in a reduction of oxidative DNA damage (indicated by oxidatively modified base 8OHG[18]) (Fig. 1g), and inhibition of DNA damage response (DDR) (indicated by phosphorylated ATM foci in cardiomyocyte nuclei) (pATM, Fig. 1h).

Next, we examined the effect of chronic hypoxia on cardiomyocyte proliferation. Chronic hypoxia induced a significant increase in heart weight to body weight ratio (Fig. 2a), although the absolute body weight did not change significantly (Extended Data Fig. 4a, top) during hypoxia, probably owing to a matched reduction in metabolic rate (Extended Data Figs 2 and 3) and food intake (Extended Data Fig. 1a). In addition, right ventricular weight (Extended Data Fig. 4a, bottom), and left ventricular weight (measured separately) were both significantly increased in hypoxic hearts (Extended Data Fig. 4a, bottom). Histological examination revealed thickening of the myocardial wall in hypoxic mice (Fig. 2b, Extended Data Fig. 4b, top). Cardiomyocyte cell size assessment using wheat germ agglutinin (WGA) staining showed that right ventricular cardiomyocyte size was significantly increased (Extended Data Fig. 4b, bottom), consistent with the effect of hypoxaemia on pulmonary artery pressure[19]. Surprisingly, we observed a significant decrease in left ventricular cardiomyocyte size following hypoxia exposure (Fig. 2c), which indicates that cardiac growth during hypoxia is not mediated by left ventricular cardiomyocyte hypertrophy. Although the mechanism of cardiomyocyte size regression is not well understood, it may partially be the result of the observed decreased mitochondrial mass, in addition to changes in sarcomere content. Next, cardiomyocytes were isolated by collagenase digestion following fixation, and the total number of rod-shaped cardiomyocytes were counted. We found that hypoxia resulted in a significant increase in the number of rod-shaped cardiomyocytes (Fig. 2d, Extended Data Fig. 4c). A similar increase was observed if both rod-shaped and round cardiomyocytes were counted (8.7×10^5 for normoxia, and 1.9×10^6 for hypoxia). This was associated with an increase in mononucleated cardiomyocytes, and a decrease in binucleated cardiomyocytes (Extended Data Fig. 4d). Next, we examined BrdU incorporation into cardiomyocyte nuclei. It is important to note that we intentionally minimized the dosage of BrdU in drinking water (0.25 mg ml^{-1}) because BrdU incorporation is known to confer more susceptibility to DNA damage[20–22]. Nonetheless, we found that hypoxic cardiomyocytes showed an eightfold increase in BrdU incorporation compared to normoxic cardiomyocytes (Fig. 2e). Moreover, we quantified the number of cardiomyocytes that were positive for the mitosis marker phosphorylated histone H3 Ser10 (pH3S10), and found that there was a significant increase in pH3S10-positive cardiomyocytes in hypoxia-exposed

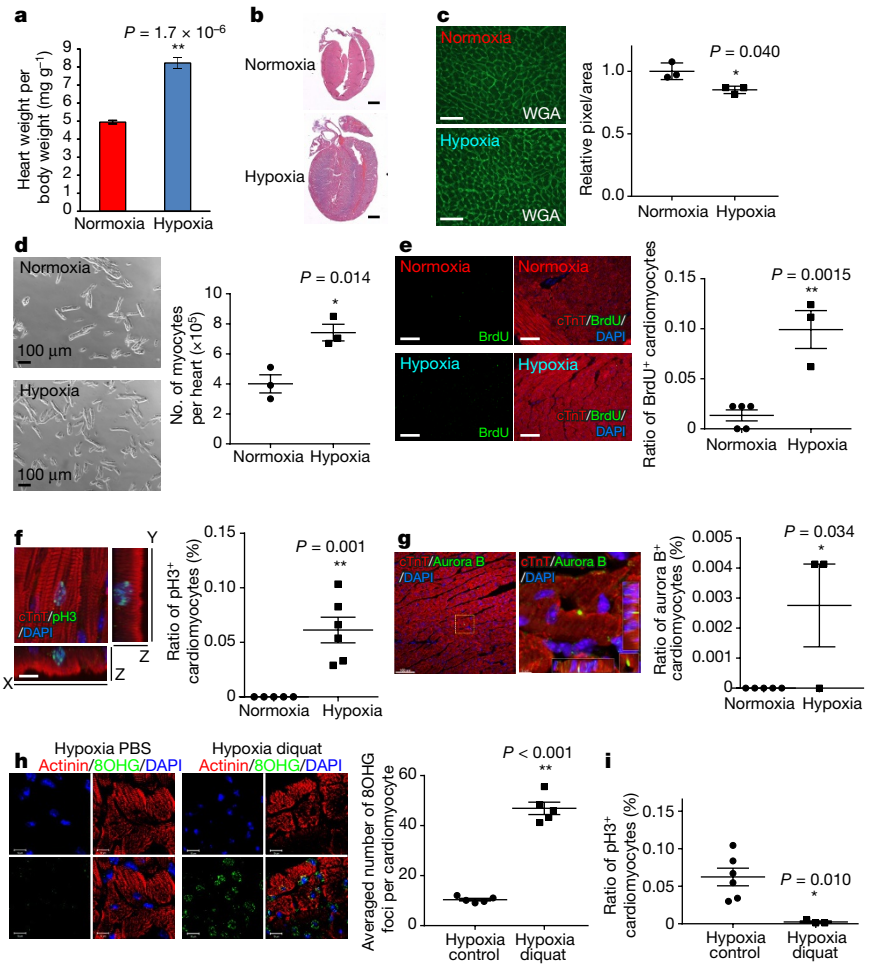

Figure 2 | Chronic hypoxia induces hyperplastic cardiac growth. a, Heart weight to body weight ratio showed a significant increase in mice exposed to hypoxia ($n = 6$ each). **b**, Haematoxylin and eosin staining showed enlarged hearts in mice exposed to hypoxia than normoxia ($n = 3$ each). **c**, Wheat germ agglutinin (WGA) staining showed significantly decreased cardiomyocyte cell size in mice exposed to hypoxia ($n = 3$ each). Scale bars, 50 μm. Cell size is measured by the average number of pixels per area surrounded by WGA (relative pixel/area). **d**, A complete dissociation of cardiomyocytes by collagenases indicated a significant increase in the total number of rod-shaped cardiomyocytes after 2 weeks of hypoxia exposure ($n = 3$ each). **e**, A significant increase in BrdU incorporation was found in hypoxia-exposed cardiomyocytes ($n = 5$ for normoxia, and 3 for hypoxia). Upper panels are lower magnification images with scale bars of 100 μm. Lower panels are higher magnification images with scale bars of 20 μm. **f**, Co-immunostaining with anti-pH3S10 and anti-cTnT antibodies showed significantly increased cardiomyocyte mitosis in mice exposed to hypoxia ($n = 5$ for normoxia, and 6 for hypoxia). Scale bar, 20 μm. **g**, Co-immunostaining with anti-aurora B and anti-cardiac troponin T (cTnT) antibodies showed increased cardiomyocyte mitosis in mice exposed to hypoxia ($n = 5$ for normoxia, and 3 for hypoxia). **h**, Diquat injection markedly increases oxidative DNA damage in hypoxic cardiomyocytes. Confocal images demonstrating 8OHG staining in control hypoxic (left) and diquat-treated (right) hypoxic cardiomyocytes ($n = 5$ each). **i**, Quantification of pH3S10$^+$ cardiomyocytes in control hypoxic and diquat-treated hypoxic cardiomyocytes demonstrating lack of cardiomyocyte mitosis in diquat-treated hypoxic cardiomyocytes ($n = 6$ for control, and 3 for diquat). Data are presented as mean ± s.e.m. $^*P < 0.05$, $^{**}P < 0.01$.

mouse hearts (Fig. 2f). In addition, we found that localization of the cytokinesis marker aurora B kinase to the cardiomyocyte cleavage furrow was significantly increased in hypoxia-treated mice (Fig. 2g). Finally, RNA-seq analysis supported the effect of hypoxia on cardiomyocyte metabolic and cell cycle changes (Extended Data Fig. 5).

Importantly, we observed a significant expansion of the population of cycling cardiomyocytes labelled by the expression of tdTomato in αMHC-CreERT2-ODD;R26/tdTomato by more than 3.6 times following 2 weeks of hypoxia (Extended Data Fig. 6a). We also observed a trend towards an increase in pH3S10$^+$/tdTomato$^+$ cardiomyocytes in hypoxic αMHC-CreERT2-ODD;R26/tdTomato hearts compared with normoxic hearts (Extended Data Fig. 6b). The total number of pH3S10$^+$ cardiomyocytes was higher in the non-tdTomato$^+$ population, indicating that previously non-proliferative cardiomyocytes are the major source of new cardiomyocyte formation. Systemic administration of the ROS generator diquat resulted in a significant increase in oxidative DNA damage in cardiomyocytes in diquat-injected mice compared with control mice (Fig. 2h). Remarkably, diquat injection inhibited the hypoxia-induced cardiomyocyte mitosis, as indicated by a marked decrease in pH3S10$^+$ proliferating cardiomyocytes (Fig. 2i).

We then examined whether this cardiomyocyte proliferation response has a role in heart regeneration. We induced MI by permanent ligation of the proximal left anterior descending (LAD) coronary artery and then exposed the mice to the same gradual hypoxia protocol by gradually reducing oxygen tension by 1% per day (Fig. 3a). After 2 weeks at 7% oxygen, mice were either euthanized and hearts were harvested, or the oxygen tension was raised again by 2% per day until ambient oxygen level was reached, after which the mice underwent echocardiographic measurement of left ventricular function and scar size assessment (Fig. 3a, c–e). We found that the ratio of heart weight to body weight in the hypoxia-treated mice was significantly increased (Fig. 3b). Histological analysis and quantification of the scar showed that the hypoxia-treated hearts had significantly smaller fibrotic scars (Fig. 3c, d). Moreover, although there was a marked reduction in left ventricular systolic function following MI in both groups (Fig. 3e), significant improvement of systolic function was observed only in the hypoxia group (Fig. 3e). Notably, the vast majority of pH3S10- or BrdU-positive cardiomyocytes were localized to the remote zone (Extended Data Fig. 6c), which may reflect the effect of wall stress in the border zone on cardiomyocyte proliferation. In a separate set of studies, exposure of MI mice to 7% oxygen for 3 weeks (Extended Data Fig. 7a) resulted in increased mortality (Extended Data Fig. 7b), although the surviving mice had significantly higher left ventricular ejection fraction compared to normoxic mice (Extended Data Fig. 7c). Assessment of pulmonary acceleration time after the recovery to ambient oxygen showed that there was no persistent pulmonary hypertension (Extended Data Fig. 7d).

Cell size analysis demonstrated that there is a significant decrease in cardiomyocyte size in the MI remote zone, but not the border zone (Fig. 3f). Moreover, we observed a significant increase in BrdU-positive cardiomyocytes (over 20-fold; Fig. 3g), as well as an increase in the number of cardiomyocytes positive for pH3S10 (Fig. 3h) and aurora B (Fig. 3i) in the hypoxia group. This was associated with a marked increase in capillary size, although the capillary density was unchanged (Fig. 4a). In addition, coronary casting revealed a remarkable enhancement of coronary collaterals in the MI hypoxia hearts (Fig. 4b), which along with cardiomyocyte proliferation supports an improvement in cardiac function following LAD ligation. In agreement with these results, we found that hypoxia was associated with a marked increase in BrdU incorporation in vascular smooth muscle cells and vascular endothelial cells (Extended Data Fig. 8).

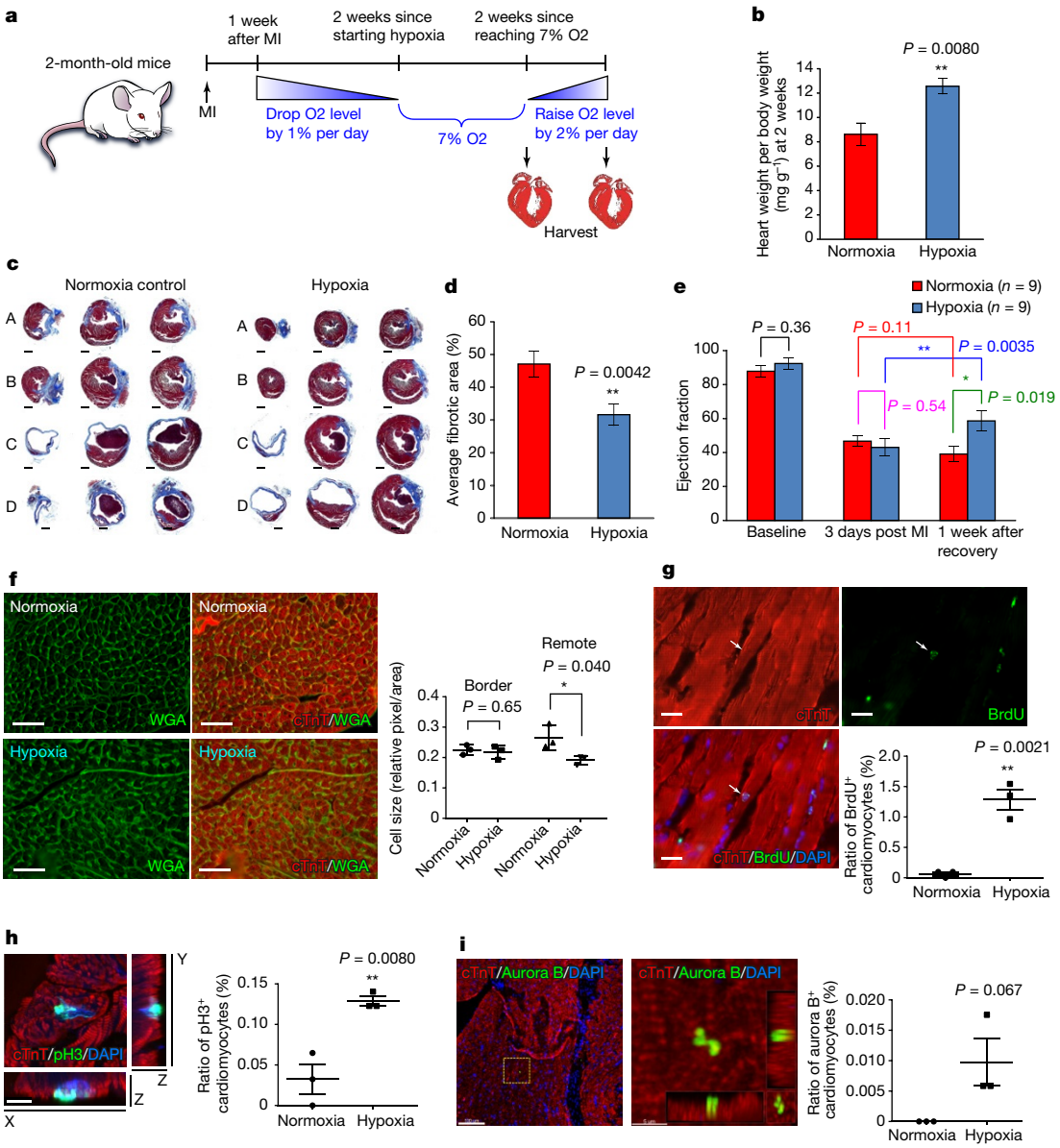

Figure 3 | Chronic hypoxia exposure induces cardiac regeneration through cardiomyocyte proliferation. a, One week after MI induced by LAD ligation, mice were exposed to gradual FiO_2 reduction to 7%, which was then maintained for 2 weeks. Mice were either euthanized, or subjected to gradual FiO_2 increase back to normoxia. **b**, Heart weight versus body weight ratio showed an increase in heart weight after 2 weeks of exposure to 7% oxygen ($n = 9$ for normoxia, and 6 for hypoxia). **c**, Trichrome staining showed less fibrotic scar in mice exposed to hypoxia. Scale bars, 1 mm. **d**, Quantification of fibrotic area relative to myocardium in trichrome-stained sections demonstrated a significant decrease in scar formation in the hypoxia-treated mice ($n = 7$ for normoxia control group and $n = 8$ for hypoxia group). **e**, Echocardiography analysis showed improved ejection fraction in hypoxia-treated mice. A bar graph shows ejection fraction at baseline, 3 days after MI and 1 week after mice were recovered to normoxia ($n = 9$ each). **f**, Wheat-germ agglutinin (WGA) staining showed no significant difference in cardiomyocyte cell size between MI mice exposed to hypoxia and normoxia in border zone, whereas a significant decrease in remote zone ($n = 3$ each). Left ventricular and septum regions were measured. Scale bars, 50 μm. **g**, Immunostaining showed significant increase in BrdU incorporation in cardiomyocytes after hypoxia exposure ($n = 3$ each). Scale bars, 20 μm. **h**, Co-immunostaining with anti-pH3S10 and anti-cTnT antibodies showed significantly increased cardiomyocyte mitosis in mice exposed to hypoxia ($n = 3$ each). Scale bars, 20 μm. **i**, Co-immunostaining with anti-aurora B and anti-cTnT antibodies showed increased cardiomyocyte mitosis in mice exposed to hypoxia ($n = 3$ each). Scale bars, 10 μm. Data are presented as mean ± s.e.m. $*P < 0.05$, $**P < 0.01$.

In pursuit of more tolerable hypoxic conditions, we tested mild hypoxia (10% oxygen) in combination with the administration of a mitochondria-specific ROS scavenger MitoTEMPO (Extended Data Fig. 9a). We observed a more modest but significant increase in heart weight to body weight ratio in 10% O_2-exposed hearts from both MitoTEMPO-injected and non-injected mice (Extended Data Fig. 9b). In addition, a decrease in cardiomyocyte size (Extended Data Fig. 9c) and a trend towards increase in the number of pH3S10$^+$ cardiomyocytes (Extended Data Fig. 9d) were observed in 10% O_2-exposed mice, suggesting the possibility of a clinically relevant beneficial effect of mild hypoxia, although this was not statistically significant. Finally, we performed a similar MI-hypoxia protocol, and exposed the mice to 10% oxygen. In support of the modest effect of mild hypoxia on cardiomyocyte proliferation, we did not observe a significant improvement in left ventricular ejection fraction (Extended Data Fig. 9e, f).

To determine the lineage origin of newly formed cardiomyocytes in the hypoxia-treated hearts, we used an αMHC-MerCreMer;R26/tdTomato genetic lineage tracing system, where tdTomato specifically

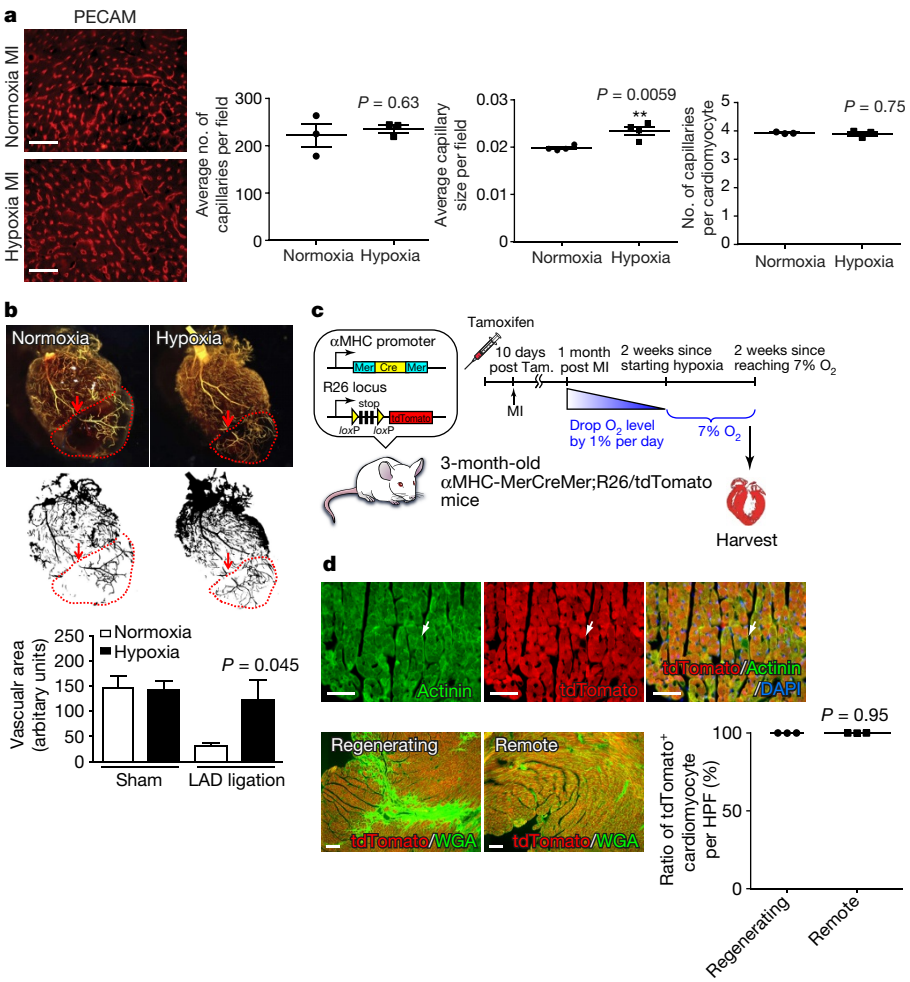

Figure 4 | Chronic hypoxia exposure induces vascular lineage and cardiomyocyte expansion. **a**, Immunostaining with endothelial markers and analysis with ImageJ revealed the enlargement of each capillary size ($n = 4$ each), but neither the density of capillaries nor average number of capillaries per cardiomyocyte was changed ($n = 3$ each). Scale bars, 50 μm. **b**, Coronary vessel casting by MICROFIL injection showed a trend in the enhancement of re-vascularization in the infarcted zone ($n = 3$ each). Vascular area, pixel density within region of interest (ROI) of binarized angiogram. Coronary vasculature was maximally dilated, pre-capillary vessels filled with MICROFIL, fixed in 4% paraformaldehyde, optically cleared, and the anterior plane imaged. ROI (red line) drawn on angiogram of each heart to delineate border zone-to-apex in same anterior plane of view, and same anatomic area in sham-ligated hearts. Arrow, point of ligation. **c**, Left panel represents a genetic mouse model of tamoxifen-dependent and cardiomyocyte-specific irreversible labelling with fluorescent protein tdTomato. Right panel shows time course of fate-mapping experiment. **d**, Top panels, immunostaining of cardiomyocyte (α-actinin) and tdTomato in border zone. Arrows indicate rare tdTomato-negative cardiomyocytes. Scale bars, 20 μm. Bottom panels, low-magnification images of tdTomato/wheat germ agglutinin (WGA) immunostaining demonstrating that the majority of cardiomyocytes are labelled with tdTomato. Bar graph shows no significant difference in ratio of tdTomato$^+$ cardiomyocytes in the injury or remote zones, indicating that newly formed cardiomyocytes are largely derived from pre-existing cardiomyocytes ($n = 3$). HPF, high-power field (×10). Data are presented as mean ± s.e.m. $^*P < 0.05$, $^{**}P < 0.01$.

and irreversibly labels cardiomyocytes upon tamoxifen induction (Fig. 4c). We observed no change in the number of tdTomato$^+$ cardiomyocytes upon exposure to 7% oxygen for 3 days without tamoxifen induction in αMHC-MerCreMer;R26/tdTomato mice (Extended Data Fig. 10), indicating that there is no increase in leakiness as a result of hypoxia exposure. Lineage tracing studies were performed where MI was induced 10 days after tamoxifen administration (Fig. 4c), and mice were subsequently exposed to the same hypoxia protocol (Fig. 4c). We found that the vast majority of cardiomyocytes were tdTomato$^+$ both in the regenerating zone (below or around the ligature) and in the remote zone (Fig. 4d). We also found very rare tdTomato$^-$ cardiomyocytes (<0.01%) both in the regenerating zone and the remote zone, which was not statistically significant (Fig. 4d). These results suggest that the majority of newly formed cardiomyocytes were derived from pre-existing cardiomyocytes.

Differentiated cardiomyocytes have long been thought to be permanently withdrawn from the cell cycle, however recent observations have supported the idea that cardiomyocytes in adult mammals can be stimulated to re-enter the cell cycle[2,3,23]. Notably, our results showed that environmental oxygen induces mitochondrial-dependent oxidative DNA damage, which regulates cardiomyocyte cell cycle in both neonatal and adult mammals[4,5]. However, it was unclear whether reduction in environmental oxygen can impact this process, or whether this 'trade-off' between energy efficiency and regenerative capacity can be reversed. Certainly, the notion that lack of oxygen, which is the most common cause of cardiomyopathy, can be used therapeutically to regenerate the injured heart is counterintuitive. Here we demonstrate that gradual reduction of inspired oxygen results in downregulation of mitochondrial metabolism and ROS production in adult cardiomyocytes. This was sufficient to induce cardiomyocyte mitosis in both injured and non-injured hearts, and resulted in significant functional recovery following myocardial infarction. Notably, this also resulted in increased coronary collaterals and capillary size, which may have a role in prevention of remodelling and improvement of left ventricular function. It is important to highlight here the differences between the physiological roles of ROS and their toxic effects, which are influenced by a multitude of factors including compartmentalization, level, source, and type of ROS. For example, Nox4 overexpression, which results in increased cytoplasmic H_2O_2 production, prolongs the post-natal window of cardiomyocyte proliferation[24], while mitochondrial ROS production has the opposite effect[4]. Similarly, ROS can both induce[25], and inhibit[26] the proliferation of stem cells. Therefore, it is critical to consider these discrepancies when designing ROS-targeted therapeutic strategies.

Hypoxia is a common trait of several regenerative organisms[4], and is required for maintenance of proliferative competency of numerous cell types[27] including cycling cardiomyocytes[5]. Although oxidative metabolism confers energy efficiency by producing higher levels of ATP compared to anaerobic glycolysis, it is becoming clear that cellular senescence and loss of endogenous regenerative properties is a price of this energy advantage. Here we show that although prolonged severe hypoxia can be poorly tolerated, it induces metabolic reprogramming of adult cardiomyocytes, resulting in cell cycle re-entry, and myocardial regeneration.

Online Content Methods, along with any additional Extended Data display items and Source Data, are available in the online version of the paper; references unique to these sections appear only in the online paper.

Received 3 March; accepted 21 October 2016.
Published online 31 October 2016.

1. Porrello, E. R. *et al.* Transient regenerative potential of the neonatal mouse heart. *Science* **331,** 1078–1080 (2011).
2. Bergmann, O. *et al.* Dynamics of cell generation and turnover in the human heart. *Cell* **161,** 1566–1575 (2015).
3. Senyo, S. E. *et al.* Mammalian heart renewal by pre-existing cardiomyocytes. *Nature* **493,** 433–436 (2013).
4. Puente, B. N. *et al.* The oxygen-rich postnatal environment induces cardiomyocyte cell-cycle arrest through DNA damage response. *Cell* **157,** 565–579 (2014).
5. Kimura, W. *et al.* Hypoxia fate mapping identifies cycling cardiomyocytes in the adult heart. *Nature* **523,** 226–230 (2015).
6. Kikuchi, K. *et al.* Primary contribution to zebrafish heart regeneration by gata4^{+} cardiomyocytes. *Nature* **464,** 601–605 (2010).
7. Poss, K. D., Wilson, L. G. & Keating, M. T. Heart regeneration in zebrafish. *Science* **298,** 2188–2190 (2002).
8. Jopling, C. *et al.* Zebrafish heart regeneration occurs by cardiomyocyte dedifferentiation and proliferation. *Nature* **464,** 606–609 (2010).
9. Adam-Vizi, V. & Chinopoulos, C. Bioenergetics and the formation of mitochondrial reactive oxygen species. *Trends Pharmacol. Sci.* **27,** 639–645 (2006).
10. Roach, R. C. & Hackett, P. H. Frontiers of hypoxia research: acute mountain sickness. *J. Exp. Biol.* **204,** 3161–3170 (2001).
11. Subramanian, R. K. *et al.* Normative data for arterial blood gas and electrolytes in anesthetized rats. *Indian J. Pharmacol.* **45,** 103–104 (2013).
12. Wise, D. R. *et al.* Hypoxia promotes isocitrate dehydrogenase-dependent carboxylation of α-ketoglutarate to citrate to support cell growth and viability. *Proc. Natl Acad. Sci. USA* **108,** 19611–19616 (2011).
13. Poleshko, A. G., Lobanok, E. S. & Volotovskii, I. D. Effect of hypoxia on porphyrin metabolism in bone marrow mesenchymal stem cells. *Bull. Exp. Biol. Med.* **157,** 167–171 (2014).
14. Vicario, C., Juanes, M. C., Martín-Barrientos, J. & Medina, J. M. Effect of postnatal hypoxia on ammonia metabolism during the early neonatal period in the rat. *Biol. Neonate* **57,** 119–125 (1990).
15. Löffler, M. The "anti-pyrimidine effect" of hypoxia and brequinar sodium (NSC 368390) is of consequence for tumor cell growth. *Biochem. Pharmacol.* **43,** 2281–2287 (1992).
16. Skappak, C., Regush, S., Cheung, P. Y. & Adamko, D. J. Identifying hypoxia in a newborn piglet model using urinary NMR metabolomic profiling. *PLoS One* **8,** e65035 (2013).
17. Mullen, A. R. *et al.* Oxidation of alpha-ketoglutarate is required for reductive carboxylation in cancer cells with mitochondrial defects. *Cell Reports* **7,** 1679–1690 (2014).
18. Kasai, H. & Nishimura, S. Hydroxylation of the C-8 position of deoxyguanosine by reducing agents in the presence of oxygen. *Nucleic Acids Symp. Ser.* **12,** 165–167 (1983).
19. Kobs, R. W., Muvarak, N. E., Eickhoff, J. C. & Chesler, N. C. Linked mechanical and biological aspects of remodeling in mouse pulmonary arteries with hypoxia-induced hypertension. *Am. J. Physiol. Heart Circ. Physiol.* **288,** H1209–H1217 (2005).
20. Djordjevic, B. & Szybalski, W. Genetics of human cell lines. III. Incorporation of 5-bromo- and 5-iododeoxyuridine into the deoxyribonucleic acid of human cells and its effect on radiation sensitivity. *J. Exp. Med.* **112,** 509–531 (1960).
21. Saffhill, R. & Ockey, C. H. Strand breaks arising from the repair of the 5-bromodeoxyuridine-substituted template and methyl methanesulphonate-induced lesions can explain the formation of sister chromatid exchanges. *Chromosoma* **92,** 218–224 (1985).
22. Morris, S. M. The genetic toxicology of 5-bromodeoxyuridine in mammalian cells. *Mutat. Res.* **258,** 161–188 (1991).
23. Malliaras, K. *et al.* Cardiomyocyte proliferation and progenitor cell recruitment underlie therapeutic regeneration after myocardial infarction in the adult mouse heart. *EMBO Mol. Med.* **5,** 191–209 (2013).
24. Murray, T. V. *et al.* Redox regulation of cardiomyocyte cell cycling via an ERK1/2 and c-Myc-dependent activation of cyclin D2 transcription. *J. Mol. Cell. Cardiol.* **79,** 54–68 (2015).
25. Le Belle, J. E. *et al.* Proliferative neural stem cells have high endogenous ROS levels that regulate self-renewal and neurogenesis in a PI3K/Akt-dependant manner. *Cell Stem Cell* **8,** 59–71 (2011).
26. Takahashi, A. *et al.* Mitogenic signalling and the p16^{INK4a}–Rb pathway cooperate to enforce irreversible cellular senescence. *Nat. Cell Biol.* **8,** 1291–1297 (2006).
27. Perales-Clemente, E., Folmes, C. D. & Terzic, A. Metabolic regulation of redox status in stem cells. *Antioxid. Redox Signal.* **21,** 1648–1659 (2014).

Acknowledgements We thank the McDermott Center Sequencing and Bioinformatics Cores for sequencing and analysis, J. Richardson and J. Shelton for assistance with histology, G. Jay for assistance with the hypoxia protocol, K. Nham for help with coronary imaging and A. Darehshouri for assistance with electron microscopy. This work is supported by the NIH (grant 1R01HL115275-01) (H.A.S.), and Center for Regenerative Science and Medicine. C.X.S. was partially supported by NIH grant UL1TR001105. A.M.S. is supported by the British Heart Foundation (CH/1999001/11735).

Author Contributions Y.N., D.C.C. and W.K. designed and performed the experiments and wrote the manuscript. Y.N., D.C.C., W.K. and H.A.S. analysed the data. S.T. performed experiments related to animal husbandry as well as various immunohistochemical studies. S.A. and A.A. performed confocal imaging quantification and studies. C.X.S. and A.M.S. performed mass-spectrometry-based analysis and quantification. H.Z. and J.E.F. performed coronary casting and the data analysis. M.T.K. and L.I.S. performed mitochondrial function and mass spectrometry analysis of metabolic enzymes. C.X. supervised the analysis of RNA-seq studies. R.J.D. and Z.H. performed metabolite measurements and data analysis. O.O. contributed coronary imaging. Z.L. performed RNA sample preparation for RNA-seq. C.C.Z. designed and supervised RNA-seq studies. J.A.H. and G.S. acquired and analysed pulmonary artery acceleration time data. H.A.S. conceived the project, contributed to experimental design and manuscript preparation. All authors approved the manuscript.

Author Information Reprints and permissions information is available at www.nature.com/reprints. The authors declare no competing financial interests. Readers are welcome to comment on the online version of the paper. Correspondence and requests for materials should be addressed to W.K. (wataru.kimura@utsouthwestern.edu) or H.A.S. (hesham.sadek@utsouthwestern.edu).

Reviewer Information *Nature* thanks R. Lee and the other anonymous reviewer(s) for their contribution to the peer review of this work.

METHODS

Animals. All protocols were approved by the Institutional Animal Care and Use Committee of the University of Texas Southwestern Medical Center. All experiments were performed on age-matched male mice. C57BL/6J mice were used for wild-type studies. R26R-tdTomato (B6:129S6-*Gt(ROSA)26Sor*$^{tm9(CAG\text{-}tdTomato)}$ Hze/J) and αMHC-MerCreMer (Tg(Myh6-Cre/Esr1*)1Jmk) mice were obtained from the Jackson Laboratory.

Histology. Hearts were harvested and fixed in 4% paraformaldehyde (PFA)/PBS solution overnight at room temperature and then processed for either paraffin or cryo embedding. Masson's trichrome staining was performed according to standard procedures at UTSW core histology facility on paraffin sections.

Murine model of myocardial infarction. Induction of anterior wall myocardial infarction (MI) was undertaken using a protocol previously established by the Sadek Laboratory[1,28]. Three-month-old adult male mice were subjected to MI by ligation of the proximal aspect of the left anterior descending (LAD) coronary artery. In brief, mice were anaesthetized in an airtight chamber using 5% isofluorane, endotracheally intubated, and ventilated using a volume controlled ventilator with 100% O_2, supplemented with 2% vaporized isofluorane (Harvard Apparatus). Following lateral thoracotomy and pericardiectomy, the LAD coronary artery was identified along the anterior wall of the left ventricle. Using a 7-0 prolene suture, the LAD artery was ligated at the proximal portion of the artery, close to its origin with the left main coronary artery. Occlusion of the LAD artery resulted in immediate blanching of the anterior wall of the left ventricle indicative of myocardial ischaemia. Subsequently, the chest was closed in layers using 5-0 silk sutures and the skin was closed using adhesive glue, Vetbond (3M). Subsequently, the mouse was extubated and allowed to recover from surgery under a heating lamp.

Echocardiography. Assessment of *in vivo* cardiac function on conscious, non-sedated mice was performed with the Vevo 2100 micro-ultrasound system (VisualSonics) at baseline, 3 days post injury, and at the end of study.

Echocardiographic M-mode images were obtained from a parasternal short-axis view. Echocardiography performed 3 days post MI demonstrated a severe reduction in left ventricular ejection fraction (LVEF). Echocardiography was then performed upon completion of the study after the hypoxia mice had returned to normoxia. LVEF was calculated at all time points.

Pulmonary artery acceleration time. Transthoracic echocardiography was performed using a Vevo 2100 imagining system under light general anaesthesia using isoflurane. 2D images were acquired of the pulmonary valve, and pulsed-wave Doppler recordings were obtained from just below the pulmonary valve. Measurements were performed blinded to the condition of the mice. All measurements were averaged over five cardiac cycles.

Mitochondrial DNA quantification and christae density. qPCR analysis for mitochondrial DNA has been published previously[4]. In brief, DNA was purified from freshly frozen ventricles (ventricles from three hearts were pooled) with Proteinase K digestion and subsequent phenol/chloroform extraction. Mitochondrial DNA (mtDNA) was quantified with SYBR green PCR Master Mix and 7000 Sequence Detection System (Applied Biosystems). Primers used are following: mtND1 forward, 5′-CTCTTATCCACGC TTCCGTTACG-3′; mtND1 reverse, 5′-GATGGTGGTACTCCCGCTGTA-3′; mtND2 forward, 5′-CCCATTCCACTTCTGATTACC-3′; mtND2 reverse, 5′-ATGATAGTA GAGTTGAGTAGCG-3′; *H19* forward, 5′-GTACCCACCTGTCGTCC-3′; *H19* reverse, 5′-GTCCACGAGACCAATGACTG-3′; *Mx1* forward, 5′-GACATAAGGTTAGCAGCTAAAGGATCA-3′; *Mx1* reverse, 5′-TCTCCGA TTAACCAGGCTAGCTAT-3′. The relative mtDNA copy number was calculated from the ratio of mtDNA copies to nuclear DNA copies. The relative fold change was then calculated based on the $\Delta\Delta C_t$ method. Cristae density was measured as previously reported[4].

NADH oxidase assay. Hearts were minced and homogenized in 6 ml of homogenization buffer (10 mM MOPS, 1.0 mM EDTA, 210 mM mannitol, and 70 mM sucrose, pH 7.4) using a Polytron homogenizer (low setting, 3 s). The homogenate was centrifuged at 500*g* for 5 min (4 °C), and the supernatant was filtered through cheese cloth. Heart homogenate was diluted to 35 μg ml^{-1} in 25 mM MOPS, 10 mM KCl at pH 7.4. NADH-supported electron transport was assessed spectrophotometrically as the rate of NADH consumption (340 nm, $\varepsilon = 6{,}200\ M^{-1}\ cm^{-1}$) following addition of 100 μM NADH. Rotenone (1.0 μM), a complex I inhibitor, was added to determine the specificity of the assay.

Reactive oxygen species measurement. Dihydrorhodamine 123 (Life Technologies, D-23806) was reconstituted in DMSO. Freshly made cryosections of unfixed hearts were incubated in 10 μM dihydrorhodamine 123 in PBS for 30 min in dark at 37 °C and then washed with PBS and mounted with Vectashield. For HPLC-based measurement of ROS, 3–5 mg of heart tissue pieces were collected either in the chamber from the hypoxic heart or in ambient air from the control normoxic heart. DHE incubation and HPLC-based detection of specific DHE oxidation products were performed as described previously[4].

Drug administration. Tamoxifen (Sigma) was dissolved in 90% sesame oil (Sigma)/10% ethanol and stored at −20 °C. Prior to intraperitoneal (IP) injection (1 mg per day per mouse), tamoxifen solution was heated at 55 °C for 10 min. 5-bromo-2′-deoxyuridine (BrdU, 0.25 mg ml^{-1}, MP Biomedical) was introduced in the drinking water from the first day of the drop in oxygen tension until the end of 7% oxygen exposure. MitoTEMPO (Sigma) was dissolved in PBS and injected IP (0.7 mg kg^{-1}) once a day for 2 weeks since the oxygen tension reached 7% to the end of 7% oxygen exposure. Diquat (diquat dibromide monohydrate, Fluka, 8 mg kg^{-1}) was dissolved in PBS and injected IP twice a week[4] for two weeks from the first day to drop the oxygen tension to the final target of 7% oxygen exposure.

Wheat germ agglutinin staining and quantify cell size. For antigen retrieval, the slides were boiled in citrate buffer (BioGenex) for 20 min, followed by cooling down for 30 min in a water container then washed three times with PBS. The slides were permeabilized with 0.3% Triton X, washed with PBS three times, and incubated with wheat germ agglutinin (WGA) conjugated to Alexa Fluor 488 (50 mg ml^{-1}, Life Technologies) for 1 h at room temperature. The slides were washed with PBS three times and mounted in antifade mounting medium (Vector Laboratories, Burlingame, California). To quantify the cell size, three independent samples per group with three different fields and positions, each from left and right ventricles, and septum were captured at 40× magnification. ImageJ (National Institutes of Health) was used to quantify the size of each cell.

Immunostaining. Tissues were fixed in 4% paraformaldehyde in PBS for either 1 h at room temperature or overnight at 4 °C and sunk in 30% sucrose in PBS at 4 °C overnight. Tissues were embedded in tissue freezing medium and cut 8 μm thickness. For antigen retrieval, either 1 mM EDTA with 0.05% Tween 20 in boiling water or epitope retrieval solution (IHC World) in a steamer (IHC-Tek Epitope Retrieval Streamer Set) were used, then sections were blocked with 10% serum from the host animal of secondary antibodies, and incubated with primary antibodies overnight at 4 °C. The sections were subsequently washed with PBS and incubated with corresponding secondary antibodies conjugated to Alexa Fluor 488 or 555 (Invitrogen). The slides were mounted in antifade mounting medium (Vector Laboratories, Burlingame, California). Primary antibodies used are following: anti-phospho histone H3 Ser10 (Millipore 06-570, 1:100), anti-aurora B (Sigma A5102, 1:100), anti-troponin T, cardiac isoform Ab-1, clone 13-11 (Thermo Scientific MS-295-P1, 1:100), anti-bromodeoxyuridine (Roche 11170376001, 1:25), anti-sarcomeric α-actinin (Abcam, ab68167, 1:100), anti-oxoguanine 8 (Abcam Ab64548, 1:25), anti-8 hydroxyguanosine (Abcam ab62623, 1:50), anti-phosphorylated ATM (Santa Cruz Biotechnology sc-47739, 1:100), anti-DsRed (Santa Cruz Biotechnology sc-33354, 1:100), anti-SM22α (Abcam ab14106, 1;100), anti-IsoB4 (Vector Laboratories FL-1201) and anti-BrdU (Abcam ab92827, 1:300). DAPI was used for the nuclear staining.

Cardiomyocyte isolation. The isolation of cardiomyocytes was performed as previously described[28]. In brief, fresh normoxia and hypoxia adult hearts were harvested and immediately fixed in 4% PFA at 4 °C overnight. Samples were subsequently incubated with collagenase D (2.4 mg ml^{-1}, Roche) and B (1.8 mg ml^{-1}, Roche) for 12 h at 37 °C. The supernatant was collected and spun down (500 r.p.m. for two minutes) to yield the isolated cardiomyocytes. The hearts were minced to smaller pieces and the procedure was repeated until no more cardiomyocytes were dissociated from the tissue. The cardiomyocytes were stained with DAPI for nucleation counts. The haemocytometer was used for counting cardiomyocytes ($n = 3$ each).

Coronary visualization and quantification. Mice were anesthetized with ketamine/xylazine, euthanized 5 min after heparinization (10 units, IP) by thoracotomy, cannulated retrograde via the descending thoracic aorta, and the vasculature cleared by perfusion at 100 mm Hg pressure for 5 min with 100 μM sodium nitroprusside in PBS for maximal dilation. Yellow Microfil^{R} (8:1:1, latex:diluent:curing agent; Flow Tech, Carver, MA) was infused via the cannula while viewing the coronary circulation with a surgical microscope. Injection was continued until the distal LAD was filled to the point of ligation. After curing for at least 20 min while maintaining infusion pressure, the heart was fixed overnight in 2% PFA, dehydrated through an alcohol gradient (25, 50, 75, 95, 100%), and cleared in methyl salicylate during gentle agitation. The vasculature was imaged with a Leica M205 fluorescent stereomicroscope. Regions of interest (ROI) were drawn to delineate the infarct zone or equivalent in sham-ligated animals. Binarized images were analysed for grey-level intensity by ImageJ software and expressed as vascular density (arbitrary units per μm^2).

Hypoxia chamber. O_2 control glove boxes and cabinets (COY laboratory) were used for animal studies. O_2 cabinets with manual purge airlock were installed with glove boxes, oxygen control system with an oxygen sensor, a nitrogen and oxygen gas regulator, gloveless sleeves and arm port plugs, an internal circulation

fan, and compact dehumidifier. Automatic filtration system with activated charcoal (Acurel LLC Economy Activated Filter Carbon Pellets) and CarboLime carbon dioxide absorbent (Bay Medical, 7-1201-20) were used for the removal of CO_2 and ammonia. Age-matched male C57/B6 mice, αMHC-CreERT2-ODD;R26/tdTomato mice or αMHC-MerCreMer;R26/tdTomato mice were exposed to the hypoxic or normoxic environment. For hypoxic environment, oxygen concentration was gradually decreased from normoxia (20.9%) to 7% oxygen concentration (1% down per day). Before exposing mice to the hypoxic environment, myocardial infarct (MI) mice were kept in normoxic condition for at least 1 week after surgery. MI mice were exposed to 7% oxygen for two weeks or longer following gradual reduction of oxygen by 1% per day. Mice were then either euthanized and hearts harvested at the end of the hypoxia experiment, or they were returned back to normoxia by increasing FiO_2 by 2% per day.

Short-run SDS–PAGE and in-gel tryptic digestion. Detailed method was described previously[4]. Briefly, freshly frozen hearts were minced and homogenized in 1.0 ml of ice-cold homogenization buffer (25 mM MOPS, 1.0 mM EDTA, pH 7.4) using a Polytron homogenizer. Total heart homogenate was then sonicated and frozen at −80 °C. Protein concentration was determined using bicinchoninic acid method (Pierce) using bovine serum albumin as a standard.

Liquid chromatography-tandem mass spectrometry. TSQ Vantage triple quadrupole mass spectrometry system (ThermoScientific) with a splitless nanoflow HPLC system with autoinjector (Eksigent) was used for LC-tandem MS. A 10 cm C18 column (Phenomenex Jupiter) packed in a fused silica electrospray tip (New Objective) was used. Detailed settings and conditions were described previously[4].

RNA sequencing. RNA was purified from fresh tissues with Qiagen RNeasy Mini kit according to manufacturer's instruction and reverse-transcribed. The cDNA was sonicated using the Covaris S2 ultrasonicator, and libraries were prepared with the KAPA High Throughput Library Preparation Kit. Samples were end repaired, 3′ ends adenylated and barcoded with multiplex adapters. PCR amplified libraries were purified with AmpureXP beads, and validated on the Agilent 2100 Bioanalyzer. Before being normalized and pooled, samples were quantified by Qubit (Invitrogen) and then run on an Illumina Hiseq 2500 using SBS v3 reagents to generate 75-bp single-end reads. Before mapping, reads were trimmed to remove low-quality regions in the ends. Trimmed reads were mapped to the mouse genome (mm10) using TopHat v2.0.1240 with the UCSC iGenomes GTF file from Illumina. Alignments with mapping quality less than 10 were discarded. Expression abundance estimation and differential expression gene identification was done using edgeR. Genes with $\log_2$[fold change] > 2 and FDR < 0.05 were deemed significantly differentially expressed between the two conditions. Pathway analysis was conducted using DAVID v6.7 (https://david.ncifcrf.gov/). Differentially expressed gene heat maps were clustered by hierarchical clustering using R (http://www.R-project.org).

Metabolomics. Fresh heart tissue pieces (10–30 mg) were collected either from hypoxia-exposed mice in the hypoxia chamber or control normoxia mice with no dietary restriction. Metabolites were purified, measured and analysed following the method published previously[17].

Fibrotic scar area quantification. Four, each of normoxia and hypoxia myocardial infarcted (MI) mouse hearts were cryo-sectioned and processed for standard Masson trichrome staining. Fibrotic area on trichrome stained sections were quantified with ImageJ (NIH).

Capillary density and size. Tissues were treated with 0.25% Trypsin-EDTA at 37 °C for 10 min, and stained with anti-PECAM (CD31) primary antibody (BD Pharmingen 553370, 1:10) at 4 °C for two nights, followed by a secondary antibody and anti-WGA conjugated to Alexa Fluor 488 (50 mg ml^{-1}, Invitrogen) staining. Capillary density and size were analysed by ImageJ.

Data analysis. For the quantification of the number of BrdU, pH3S10 or aurora B^+ cardiomyocytes, the results acquired from sections of the heart harvested from each animal at the ventricular valve level of the four-chamber view, or at the level of ligature of the two-chamber view, with at least 100 μm distance from each other were averaged. To calculate the rate of proliferating cardiomyocytes, we stained cryosections of injured or non-injured normoxia/hypoxia sections with cTnT/WGA/DAPI and counted the total number of cardiomyocyte nuclei per section. All graphs represent average values, and all error bars represent s.e.m. All data collected and analysed were assumed to be distributed normally. No statistical methods were used to predetermine sample size. The experiments were not randomized and the investigators were not blinded to allocation during experiments and outcome assessment except for all echocardiographic studies. Student's *t*-test was used to determine statistical significance. $*P < 0.05$ and $**P < 0.01$ were considered statistically significant.

Data availability. RNA sequencing data are available from NCBI Sequence Read Archive (BioProject accession: PRJNA348637). All other data are available from the corresponding authors upon reasonable request.

28. Mahmoud, A. I. *et al.* Meis1 regulates postnatal cardiomyocyte cell cycle arrest. *Nature* **497,** 249–253 (2013).

A. Food consumption

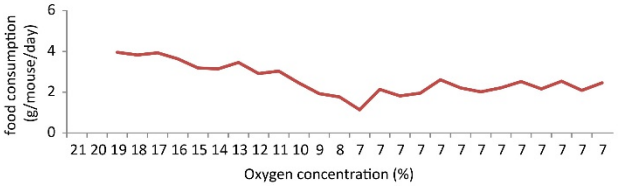

B. Blood gas

	pO2 (mmHg)	pCO2 (mmHg)	pH
Normoxia	76.2±19.1	37.3±5.05	7.24±0.0223
Hypoxia	34.3±4.30	21.8±2.68	7.17±0.0267

C. Hif activation

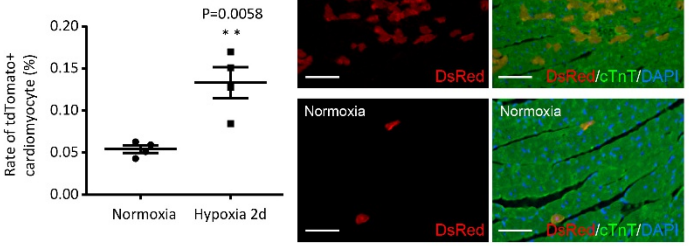

D. Mass spec

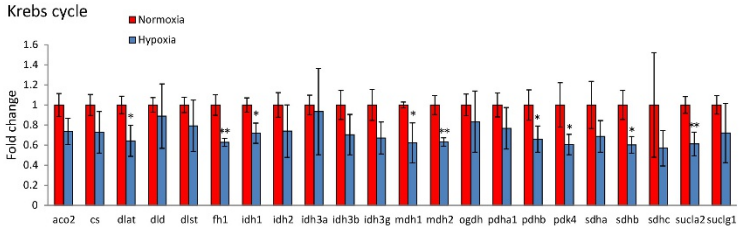

E. dihydrorhodamine 123

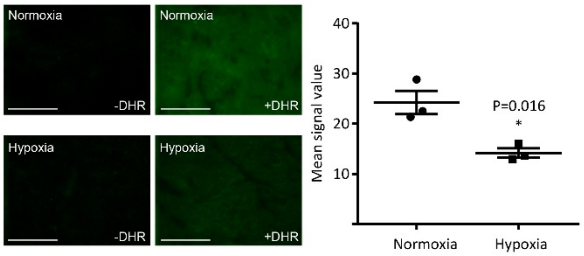

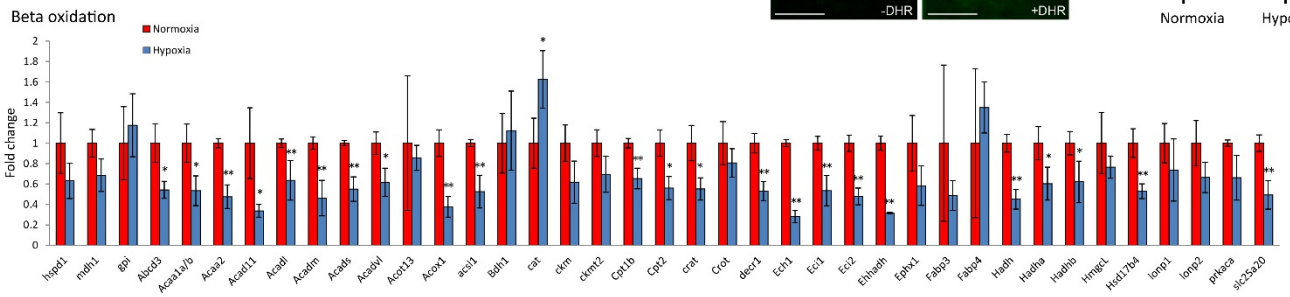

Extended Data Figure 1 | Metabolic effects of hypoxia. a, Food consumption over the course of hypoxia exposure demonstrating a gradual decline ($n = 9$). **b**, Blood gas and pH analysis ($n = 14$ for normoxia control group, and $n = 9$ for hypoxia group). **c**, Two days of exposure to 7% O_2 showed a significant increase in number of tdTomato$^+$ cardiomyocytes in αMHC-CreERT2-ODD;R26/tdTomato double reporter mice, indicating an enhancement of Hif1α stabilization ($n = 4$ each). Scale bars, 50 μm. **d**, Comprehensive quantitative mass spectrometry analysis of enzymes involved in Krebs cycle and fatty acid β oxidation ($n = 3$ each). **e**, Dihydrorhodamine 123 staining on fresh cryosections revealed a significant decrease in ROS levels in hypoxia-treated hearts ($n = 3$ each). Scale bars, 100 μm. Data are presented as mean ± s.e.m. $^*P < 0.05$, $^{**}P < 0.01$.

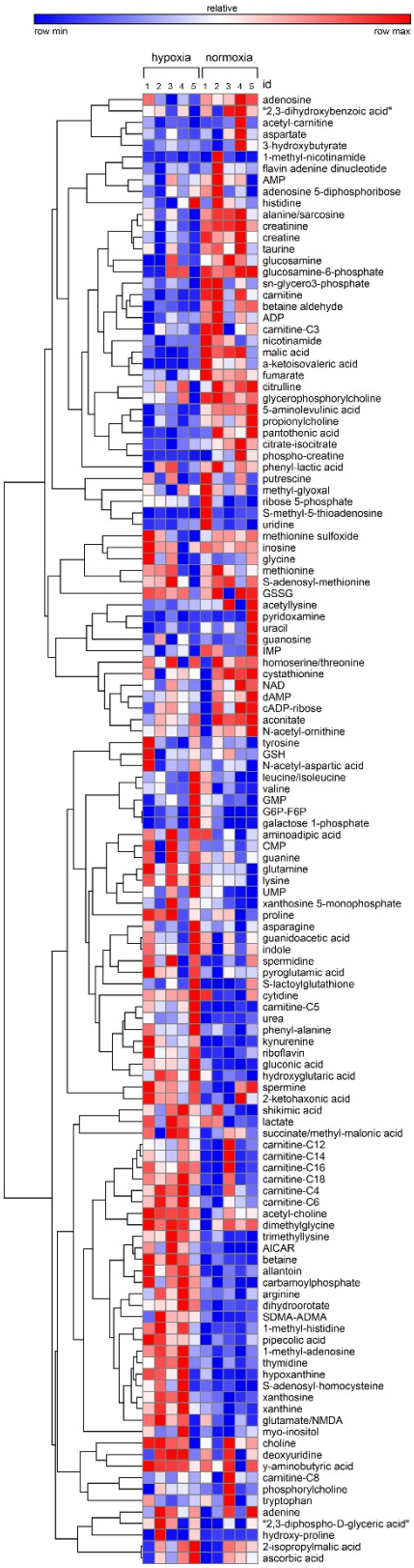

Extended Data Figure 2 | A relative abundance of metabolites extracted from quintuplicated samples of control and hypoxic heart demonstrating dysregulation of numerous pathways involved in hypoxic response ($n = 5$ each).

A. PCA

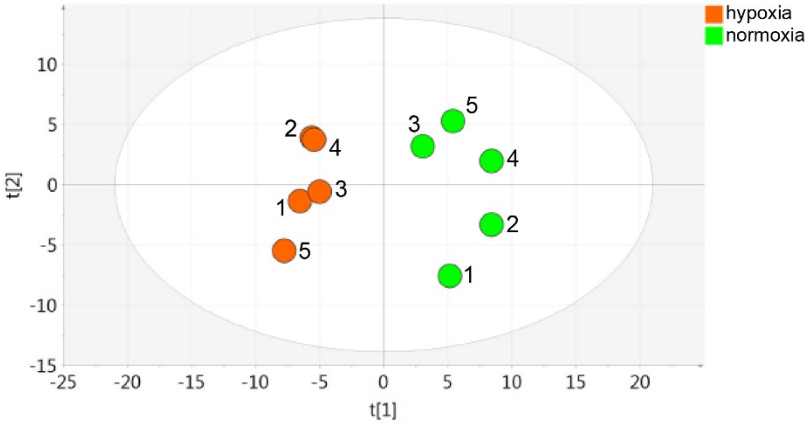

B. Pathway impact

Pathway name	Total	Hits	p
Arginin and Proline metabolism	77	10	2.27E-06
Alanine, aspartate and glutamate metabolism	24	6	6.00E-06
Purine metabolism	92	9	8.01E-05
Nitrogen metabolism	39	5	1.07E-03
Pyrimidine metabolism	60	6	1.26E-03
Aminoacyl-tRNA biosynthesis	75	6	4.00E-03
Citrate cycle (TCA cycle)	20	3	7.50E-03
Glycine, serine and threonine metabolism	48	4	1.64E-03
Pantothenate and CoA biosynthesis	27	3	1.74E-03
D-Glutamine and D-glutamate metabolism	11	2	0.021
Glycerophospholipid metabolism	39	3	0.046

Extended Data Figure 3 | Hypoxia metabolome profile. a, Principal component analysis (PCA) plot for the 10 extracts shown in Extended Data Fig. 2. **b**, The list of differentially regulated metabolic pathways in hypoxic heart compared with control normoxic hearts.

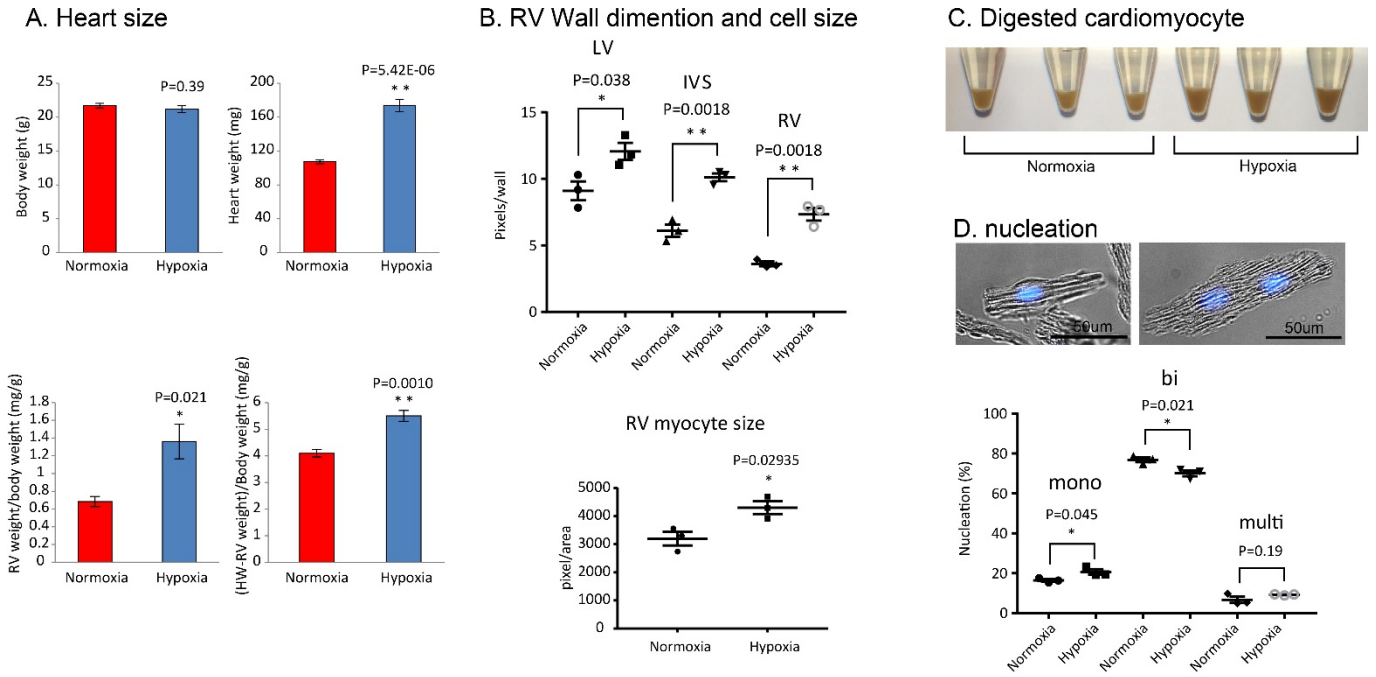

Extended Data Figure 4 | Effect of hypoxia on cardiac growth. a, Heart weight, body weight ($n = 6$ each), right ventricular weight to body weight ratio, and left ventricular and septum weight to body weight ratio ($n = 4$ for normoxia, and 5 for hypoxia) after 2 weeks of exposure to 7% oxygen. **b**, Wall dimension of right ventricular, intraventricular septum and left ventricular wall were all increased after 2 weeks of exposure to 7% oxygen ($n = 3$ each). Cardiomyocyte size in the right ventricle showed a significant increase after 2 weeks exposure to 7% oxygen ($n = 3$ each). **c**, Complete dissociation of cardiomyocytes yields a larger pellet of digested cardiomyocyte. **d**, Two weeks of exposure to hypoxia results in an increased mononucleated cardiomyocytes and reduced binucleated cardiomyocytes. Cardiomyocytes were isolated from whole ventricle ($n = 3$ each).

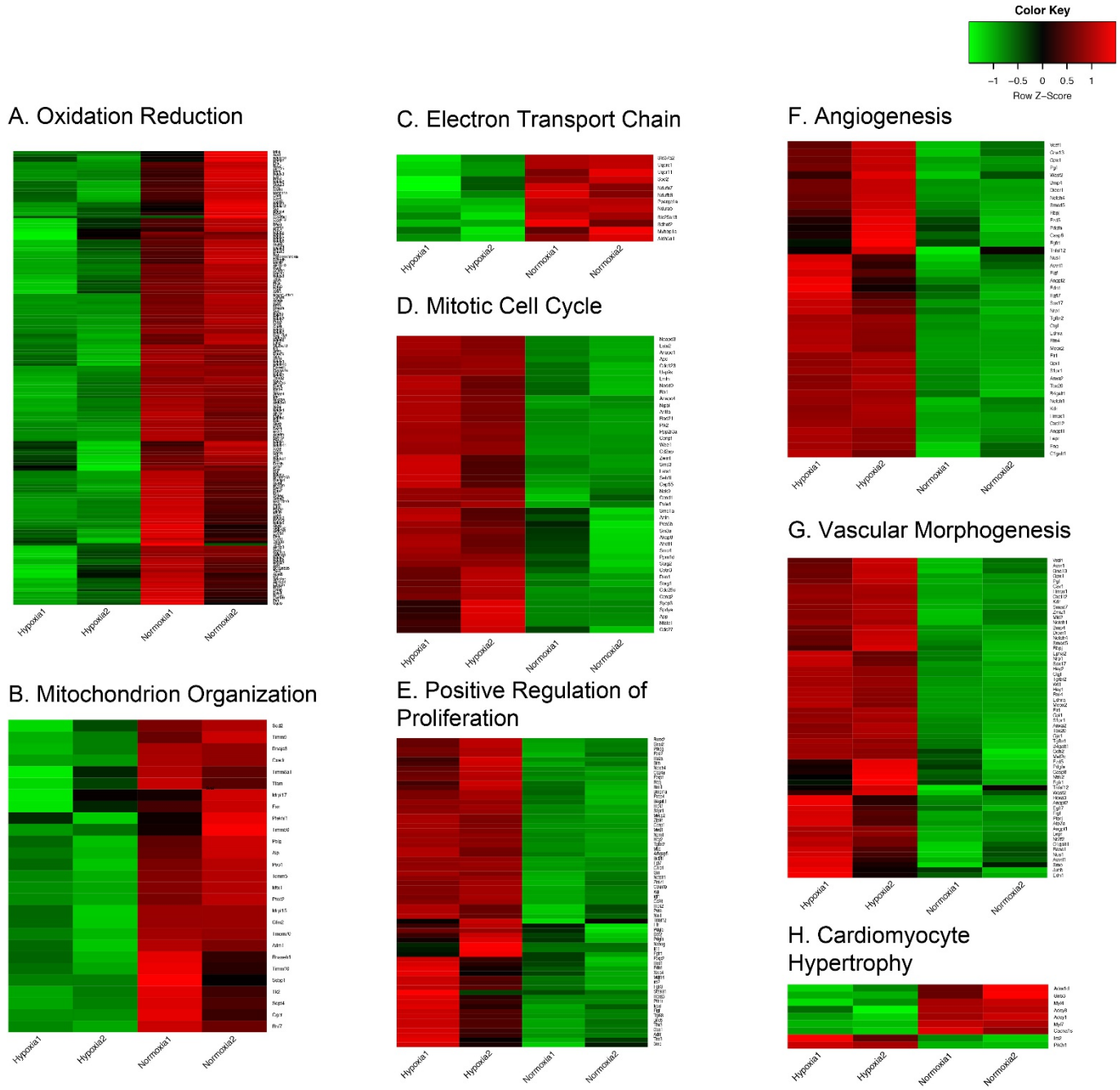

Extended Data Figure 5 | RNA-seq analysis of hypoxic and normoxic left ventricles. a–h, Ontology analysis was performed using DAVID Functional Annotation Tool. The heat maps show a number of dysregulated pathways including metabolism, cell cycle, angiogenesis and hypertrophy. Red and green colours represent upregulated and downregulated genes, respectively ($n = 2$ each duplicate).

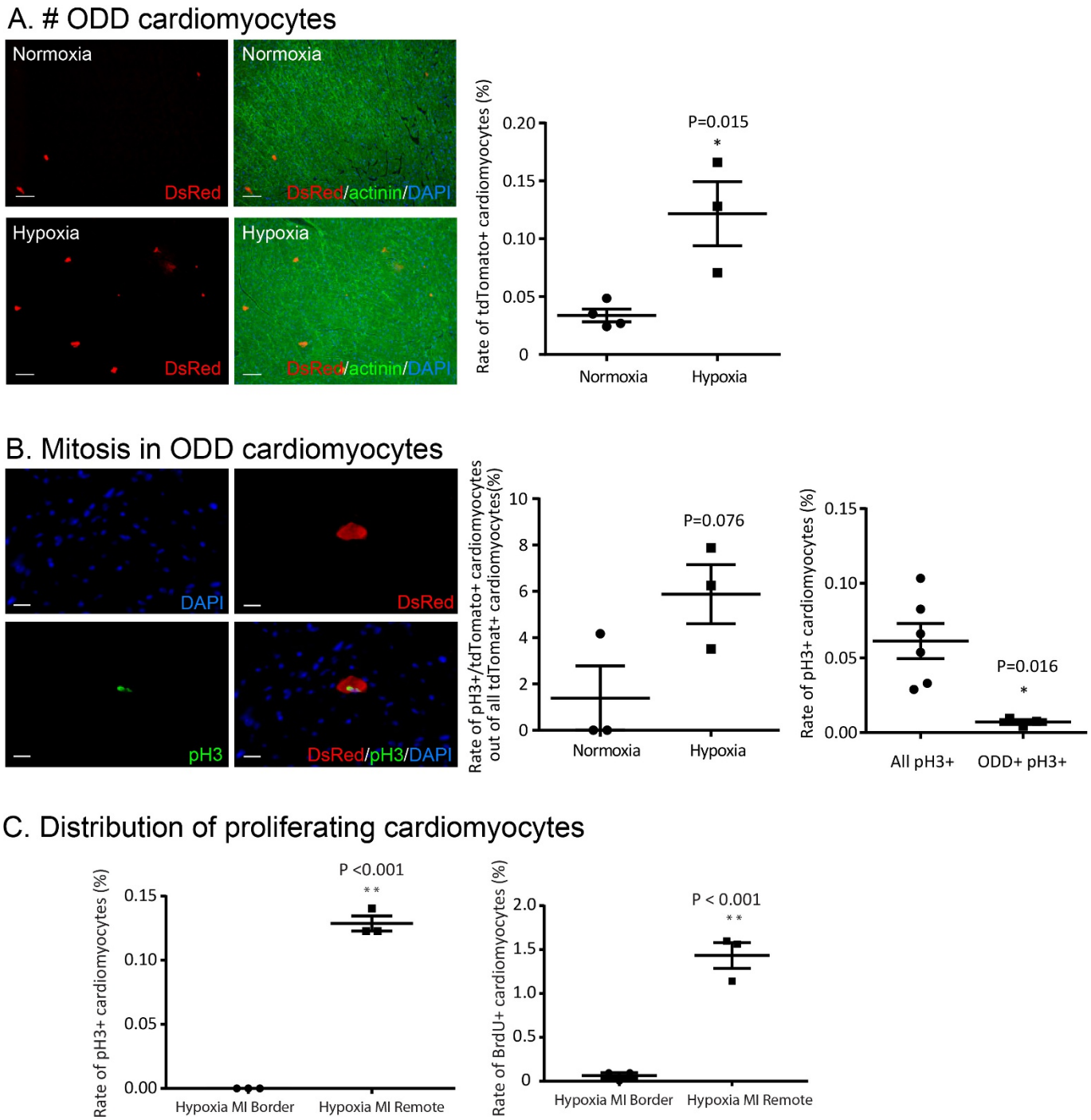

Extended Data Figure 6 | Differential effect of hypoxia on cardiomyocyte proliferation. a, Expansion of tdTomato$^+$ cardiomyocytes in αMHC-CreERT2-ODD;R26/tdTomato indicates enhancement of cell division in ODD$^+$ cardiomyocytes ($n = 4$ for normoxia, and 3 for hypoxia). Scale bars, 100 μm. **b**, The number of pH3S10/tdTomato double-positive cardiomyocytes showed an increase in hypoxic αMHC-CreERT2-ODD;R26/tdTomato transgenic mice (rate of tdTomato$^+$/pH3S10$^+$ double-positive cardiomyocytes to tdTomato$^+$ single-positive cardiomyocytes, $n = 3$ each; rate of tdTomato$^+$/pH3S10$^+$ double-positive cardiomyocytes to all pH3S10$^+$, $n = 6$ for all pH3S10$^+$, $n = 3$ for tdTomato$^+$/pH3S10$^+$ double-positive). Scale bars, 10 μm. **c**, Distribution of proliferating cardiomyocytes in the border and remote zones. The majority of pH3S10$^+$ and BrdU$^+$ cardiomyocytes were localized to the remote zone rather than the MI border zone ($n = 3$ each).

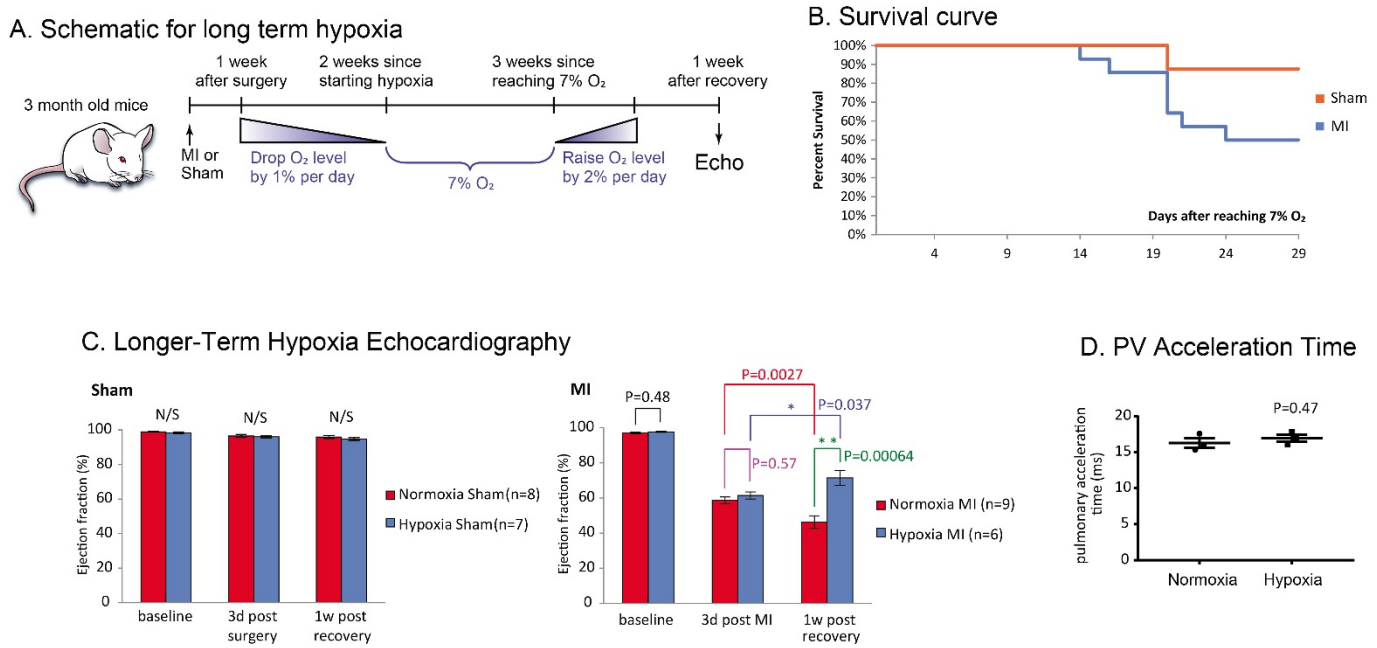

Extended Data Figure 7 | Effect of 3 weeks of hypoxia on heart regeneration. a, Schematic of 3 week hypoxia protocol. Mice were exposed to gradual FiO_2 reduction to 7% (one week following MI), which was then maintained for 3 weeks. Mice were then either euthanized, or subjected to gradual FiO_2 increase back to normoxia. **b**, Cumulative survival curve (Kaplan–Meier survival plot) of MI and sham-operated mice after reaching 7% of oxygen ($n = 8$ for sham-operated mice, and $n = 14$ for MI mice). **c**, Left ventricular function for sham and MI groups exposed to 3 weeks of 7% FiO_2 (longer duration hypoxia) ($n = 8$ for normoxia sham-operated mice, and $n = 7$ for hypoxia sham-operated mice; $n = 9$ for normoxia MI mice, and $n = 6$ for hypoxia MI mice). **d**, PVacceleration time after return to normoxia showed no evidence of pulmonary hypertension (manifested by shortened PV acceleration time) ($n = 3$ each).

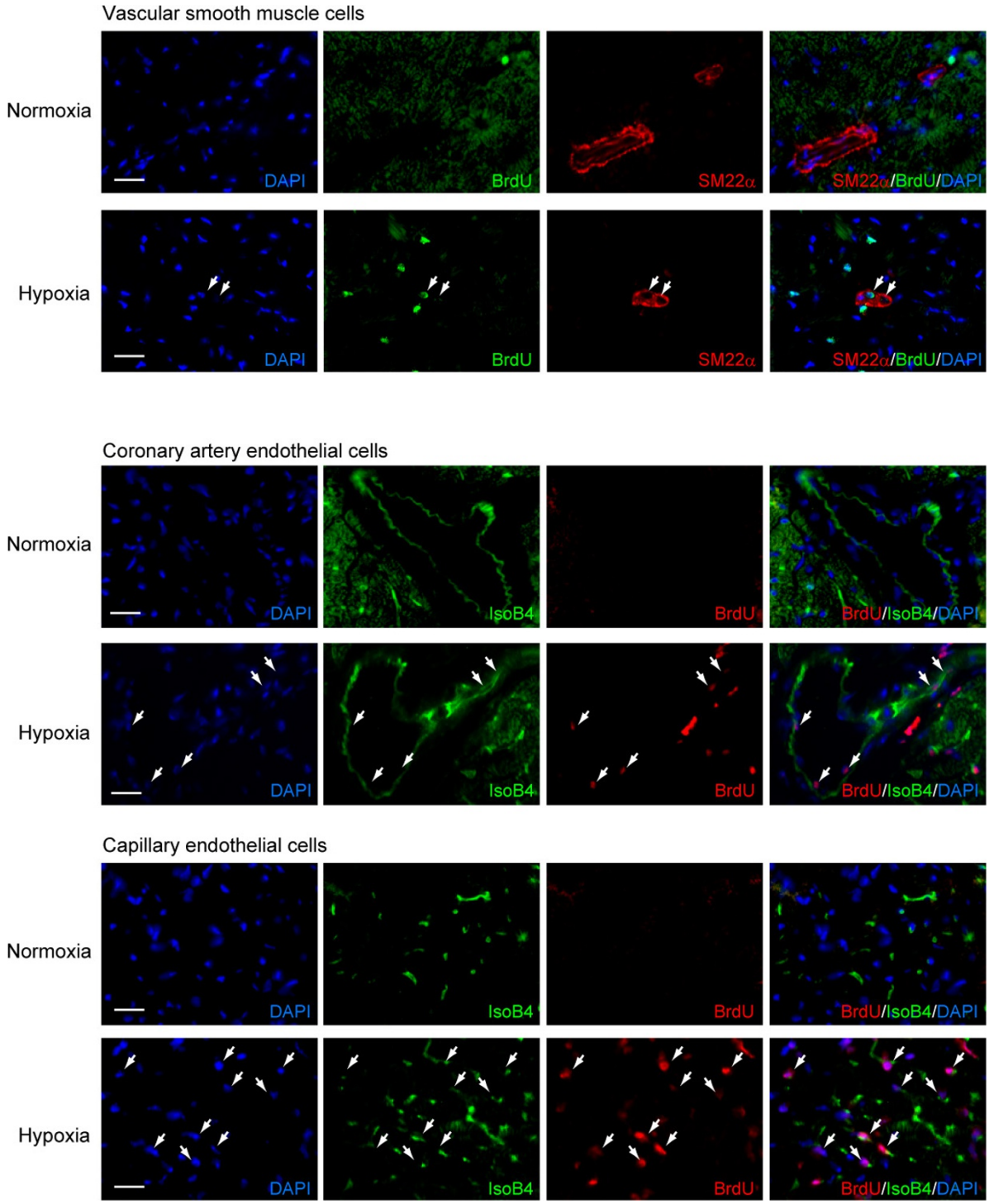

Extended Data Figure 8 | Co-immunostaining using anti-SM22α (smooth muscle cells) or FITC-conjugated isolectin B4 (endothelial cells) with an anti-BrdU antibody reveals a significant increase in BrdU incorporation in vascular lineages. Scale bars, 20 μm.

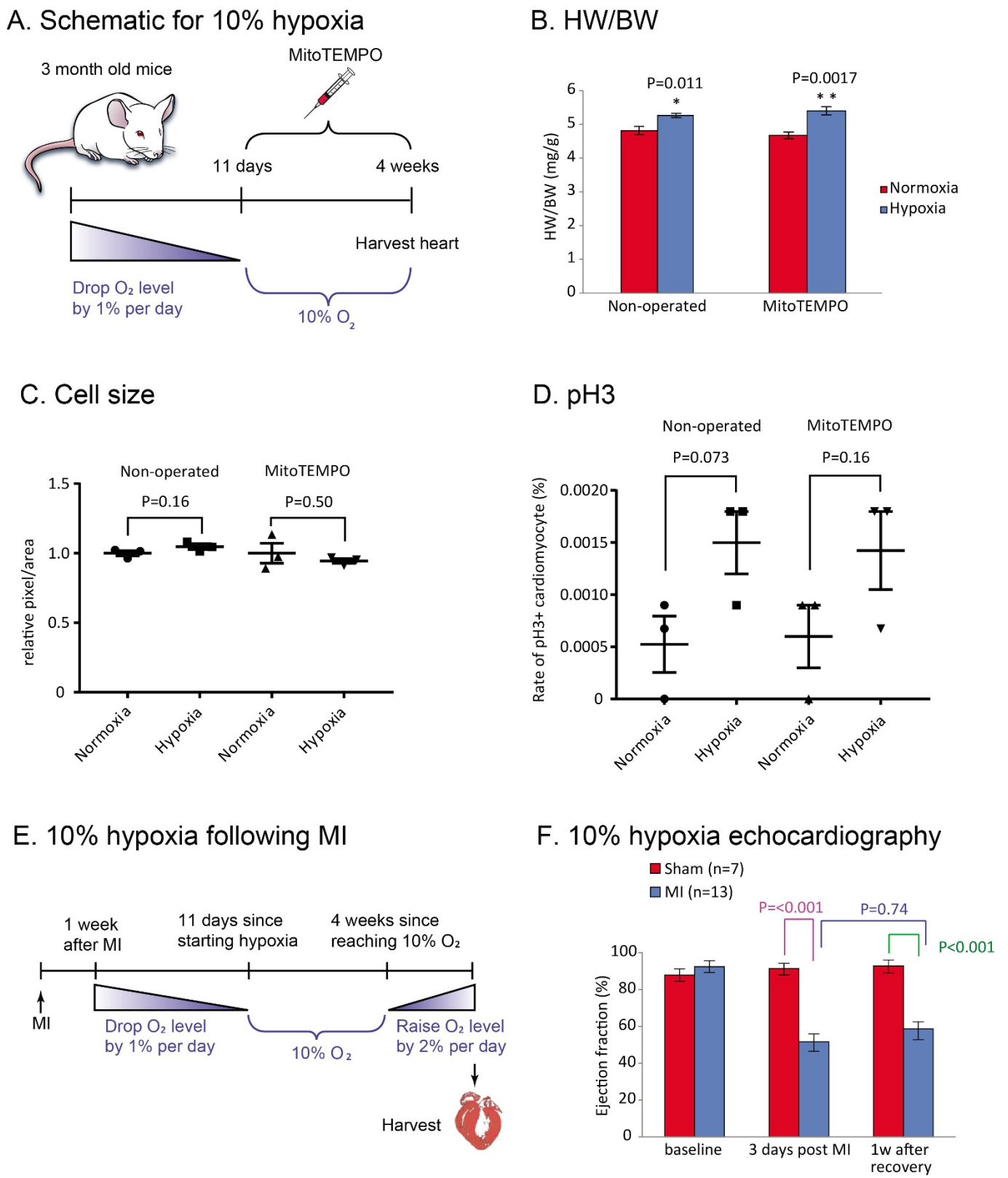

Extended Data Figure 9 | Exposure of mice to mild hypoxia (10% O_2) with or without MitoTEMPO. a, Schematic of gradual induction of mild hypoxaemia. **b**, Heart weight to body weight ratio showed a slight increase in the mild hypoxia group ($n = 5$ each). **c**, **d**, Cell size (**c**) and pH3S10 quantification (**d**) showed no significant difference between mild hypoxia and normoxia groups ($n = 3$ each). **e**, Schematic of MI followed by 10% hypoxia protocol. **f**, Echocardiography did not show significant improvement in left ventricular ejection fraction following exposure to 10% hypoxia ($n = 7$ for sham-operated mice, and $n = 13$ for hypoxia MI mice).

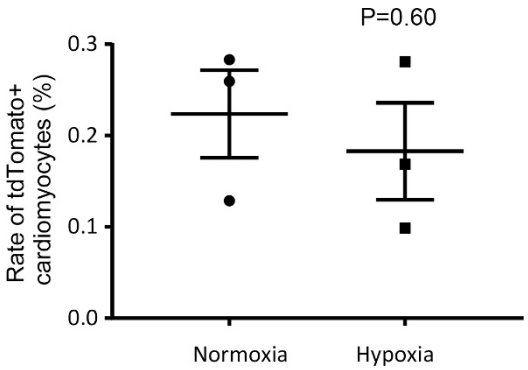

Extended Data Figure 10 | Quantification of αMHC-MerCreMer;R26/tdTomato reporter without tamoxifen pulse showing no increase in leakage during hypoxia ($n = 3$ each).